J. Electrochem. Sci. Eng. **16** (2026) 3191; https://doi.org/10.5599/jese.3191

Open Access : : ISSN 1847-9286
https://pub.iapchem.org/ojs/index.php/JESE

Original scientific paper

Influence of inevitable hydrogen evolution reaction on morphology of electrodeposited zinc

Nebojša D. Nikolić[1,✉], Jelena D. Lović[1], Nikola S. Vuković[2] and Predrag M. Živković[3]

[1]*Department of Electrochemistry, Institute of Chemistry, Technology and Metallurgy, University of Belgrade, Njegoševa 12, 11000 Belgrade, Serbia*
[2]*Institute for Technology of Nuclear and Other Mineral Raw Materials, Bulevar Franše d'Eperea 86, 11000 Belgrade, Serbia*
[3]*Faculty of Technology and Metallurgy, University of Belgrade, Karnegijeva 4, 11000 Belgrade, Serbia*

Corresponding Author: nnikolic@ihtm.bg.ac.rs; Tel.: +381-11-337-03-90; Fax: +381-11-337-03-89

Received: December 29, 2025; Accepted: February 4, 2026; Published: February 6, 2026

Abstract

Influence of parallel hydrogen evolution reaction (HER) on morphology of zinc electrodeposits has been investigated. Zn was electrodeposited potentiostatically from the alkaline electrolyte at overpotentials both inside and outside the plateau of the limiting diffusion current density, and scanning electron microscopy (SEM) was used to characterize the resulting deposits. Holes originating from detached hydrogen bubbles were formed among the branchy, fern-like dendrites at overpotentials outside the plateau of the limiting diffusion current density, while HER was not detected at the overpotential inside the plateau. The overpotential of electrodeposition had no significant effect on the amount of hydrogen produced (the HER current efficiency was in the 17.7-19.1 % range), but it did affect the hole size. Depending on the overpotential of the electrodeposition, the size of holes was from several to about 100 μm, including those obtained by a coalescence of neighbouring hydrogen bubbles, and decreased with the increasing overpotential. The absence of inhibition of dendritic growth in spite of a high value of evolved hydrogen was attributed to Zn, which belongs to the group of normal metals characterized by high values of both the exchange current density and the overpotential for hydrogen evolution.

Keywords

Electrodeposition; dendrite; crystals; holes; coalescence; SEM images.

Introduction

Environmental pollution from the massive use of fossil fuels has led to the need for the accelerated development of clean energy storage devices [1,2]. The Li-ion batteries were among the first developed renewable energy storage systems, but Li is expensive, has low energy density and its use has safety hazards. This necessitated the development of green, sustainable energy storage systems based on Na [3], Zn [4], Al [5] and K [6] that offer high safety and affordability. Among these systems, special attention is given to Zn-based rechargeable batteries, such as Zn-air, Zn-ion, Zn-Ni, and Zn-MnO_2 [1]. The development of these batteries is based on specific characteristics of Zn, including its abundance, low cost, low toxicity, and high energy storage. Also, Zn has excellent electrochemical reversibility (-0.762 V *vs*. SHE) and high capacity (5854 Ah dm^{-3} and 820 Ah kg^{-1}).

Alkaline Zn batteries are the most often used kinds of Zn-based batteries and one third of the market in the world belongs to them [7]. Neutral and mild-acid zinc electrolytes are used to a limited extent [7-11]. The biggest challenge in the development of Zn-based batteries is obtaining a stable Zn anode. The problems arising during their development are related to dendrite formation, hydrogen evolution, corrosion, passivation, and morphological variation [8,11-14]. The sharp tips of dendrites can cause a short circuit between the anode and cathode by a penetration of the separator, while the weak adhesion of dendrites is a potential cause of a loss of battery capacity due to their spontaneous detachment from the electrode surface [1,15,16]. Formation of Zn dendrites increases the specific surface area of Zn anodes, causing additionally the increase in the roughness of the anode and the number of active sites, favouring dendritic growth and a contribution of side reactions [17].

The hydrogen evolution reaction (HER) is an inevitable process in Zn electrodeposition and, hence, in Zn-based batteries. In the alkaline electrolytes, the standard reduction potential of Zn/ZnO is -1.26 V *vs*. SHE, at pH ~ 14, while that for the hydrogen evolution reaction is -0.83 V *vs*. SHE [8,12]. This means that HER is thermodynamically favoured and begins before the reduction of Zn oxide in alkaline electrolytes. Hence, HER as a parasitic reaction disables the Zn anode from being charged with 100 % current efficiency (or Coulombic efficiency), since this reaction consumes part of the electrons provided to the Zn anode during charging [15,18]. Also, the internal pressure is increased by H_2 formation from liquids to the gas phase, which strongly influences Zn electrodeposition and may damage Zn-based batteries [12,19]. Moreover, the hydrogen evolution reaction encourages local hydroxide ions to accumulate in the vicinity of the electrode, raising the pH of the electrolyte, and in that way, intensifies undesired corrosion and passivation reactions [20].

Formation and growth of dendrites from the alkaline electrolytes have been widely explored [1,8,15,21-30]. The different mechanisms, such as the "pyramid" growth model based on spiral dislocation growth controlled by bulk diffusion [31], diffusion-limited aggregation and phase-field models [32,33], a quantitative phase-field model based on Marcus kinetics theory [34], the general theory of disperse deposits formation [22,23,31,35], *etc*. are proposed to explain it. On the other hand, HER is mentioned in numerous investigations [7,8,12,15,18,19,36-39], but without insight in an influence of this reaction on the morphology of electrodeposited Zn. Bearing in mind the inevitability of HER during Zn electrodeposition, and hence, in Zn-based batteries, the aim of this study was to examine the effect of parallel HER on the morphology of Zn deposits obtained from the alkaline electrolyte.

Experimental

Electrodeposition and characterization of zinc deposits

Electrodeposition of zinc was performed potentiostatically using a BioLogic SP 200 or Parstat 4000 potentiostat and galvanostat at room temperature in an open-type cylindrical cell. The composition of the electrolyte was 28.5 g dm^{-3} ZnO in 336.7 g dm^{-3} KOH, while overpotentials of the electrodeposition were varied in the -160 to -340 mV range with a step of 60 mV, *i.e*. -160, -220, -280 and -340 mV. The electrodeposited charge was 0.75 and 1.5 mAh. The alkaline electrolyte for Zn electrodeposition was prepared from chemicals of p.a. quality and double-distilled water (18 MΩ resistivity).

The electrodeposition process was performed on cylindrical copper cathodes (length: 2.0 cm, diameter: 0.080 cm; surface area: 0.50 cm^2). The counter and the reference electrodes were of Zn. The positions of electrodes in an electrochemical cell are as follows: the counter electrode of cylindrical shape was situated around the wall of the cell, the cathode was situated in the centre of the cell, while the tip of the reference electrode was situated approximately 2.0 mm from the middle of the cylindrical part of the Cu cathode. Before the electrodeposition process, the Cu cathodes were pretreated according to the following procedure: alkaline degreasing at 70 °C, rinsing in distilled water, etching in 20 % H_2SO_4 at 50 °C, and again rinsing in distilled water as the final step of the preparation process.

The scanning electron microscope, model JEOL JSM-7001F, was used to characterize the morphology of electrolytically produced Zn deposits.

Determination of the current efficiency for hydrogen evolution reaction (HER)

Since the overall current efficiency represents a sum of the current efficiency for Zn electrodeposition, $\eta_i(Zn)$ and the current efficiency for hydrogen evolution reaction, $\eta_i(H_2)$, $\eta_i(H_2)$ can be represented by Equation (1):

$$\eta_i(H_2) = 1\,(or\ 100\,\%) - \eta_i(Zn) \tag{1}$$

where $\eta_i(Zn)$ can be defined by Equation (2) [40]:

$$\eta_i(Zn) = \frac{m_{exp}}{m_{teor}} \tag{2}$$

where m_{exp} is the mass of electrodeposited zinc with the electrodeposited charge (Q), and m_{teor} is given by Equation (3):

$$m_{teor} = \frac{Ar(Zn)Q}{n_e(Zn)F} \text{ where } Q = \int_0^t I \cdot dt \tag{3}$$

In Equation (3), Ar is the atomic mass of Zn (65.37 g mol^{-1}), $n_e(Zn)\cdot F$ is the number of Faradays per mole of consumed ions, I is the current of the electrodeposition and t is time.

The mass of electrodeposited zinc is determined according to the procedure given by Dundálek *et al.* [36]. The analytical balance with an accuracy of four decimal places is used for measuring the cylindrical copper cathodes before and after the Zn electrodeposition process with the electrodeposited charge, Q, at the selected overpotential. The difference between these two values gives the mass of electrodeposited Zn, m_{exp}. Immediately after the electrodeposition process, the cathode with electrodeposited Zn is firstly rinsed in the double distilled water and then in ethanol, left for five min at a temperature of 50 °C to evaporate any moisture and weighted.

Results and discussion

In Zn electrodeposition processes from the alkaline electrolytes, the main reactions occurring are presented by Equations (4) and (5) [36,40]:

$$[Zn(OH)_4]^{2-} + 2e^- \rightarrow Zn + 4OH^- \quad (4)$$

$$2H_2O + 2e^- \rightarrow H_2 + 2OH^- \quad (5)$$

To obtain a comprehensive insight in the effect of parallel hydrogen evolution reaction (HER) on the process of electrodeposition of Zn, the first step was to analyse the polarization characteristics of the Zn system. The polarization curve, recorded from an electrolyte containing 28.5 g dm^{-3} ZnO in 336.7 g dm^{-3} KOH by the linear sweep voltammetry technique, is shown in Figure 1. It is clear from Figure 1 that it is characterized by a clearly defined plateau of the limiting diffusion current in the range of overpotentials between -90 and -180 mV. After the plateau ended, the current increased rapidly with a further increase in overpotential.

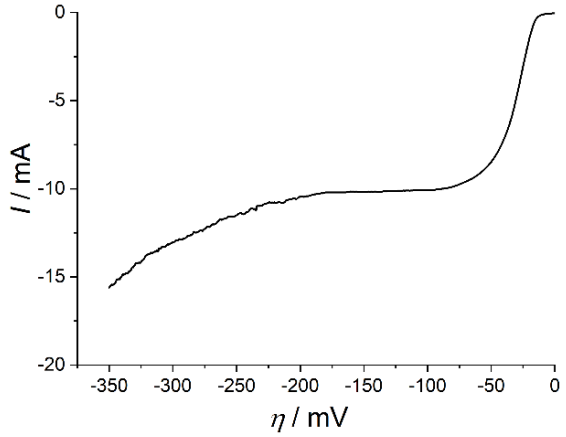

Figure 1. *Polarization curve for electrodeposition of Zn from 28.5 g dm^{-3} ZnO in 336.7 g dm^{-3} KOH. The surface area: 0.50 cm^2. Sweep rate:* v *= 1 mVs^{-1}*

The calculated values of the current efficiency for HER, $\eta_i(H_2)$, according to Equations (1) to (3) for overpotentials of the electrodeposition of -160, -220, -280 and -340 mV, are given in Table 1.

Table 1. *The values of the current efficiency for HER ($\eta_i(H_2)$), hole size (*D*) and the average current of electrodeposition (I_{av}) obtained at given overpotentials of the electrodeposition*

η / mV	$\eta_i(H_2)$ / %	D / μm	I_{av} / mA
-160	0	0	13.4
-220	17.7	100	15.6
-280	18.7	10-100	22.5
-340	19.1	up to 10	44.2

As seen from Table 1, HER was not registered at an overpotential of -160 mV, which belonged to the plateau of the limiting diffusion current density, while the $\eta_i(H_2)$ values obtained for overpotentials outside the plateau were in the range between 17.7 and 19.1 %.

The effect of overpotential of electrodeposition on morphology of Zn deposits

Figure 2 shows morphologies of Zn deposits obtained at various overpotentials, including the plateau of the limiting diffusion current density (-160 mV; Figure 2a), and those outside the plateau (-220 mV, Figure 2b; -280 mV, Figure 2c; and -340 mV, Figure 2d) with an electrodeposited charge of 1.5 mAh. The presence of HER in the Zn electrodeposits was detected by the formation of holes or craters originating from detached hydrogen bubbles, as seen from Figure 2b-2d. Simultaneously,

as expected, holes were not detected in the Zn electrodeposit obtained at an overpotential of -160 mV (Figure 2a), confirming that HER commences to occur at overpotentials outside the plateau of the limiting diffusion current density in the zone of the fast growth of current with the increase of overpotential. The dendrites of Zn of various sizes, number and a degree of ramification were formed around the holes or the craters (Figure 2b-2d), while crystals of various shapes and sizes were formed at an overpotential of -160 mV (Figure 3).

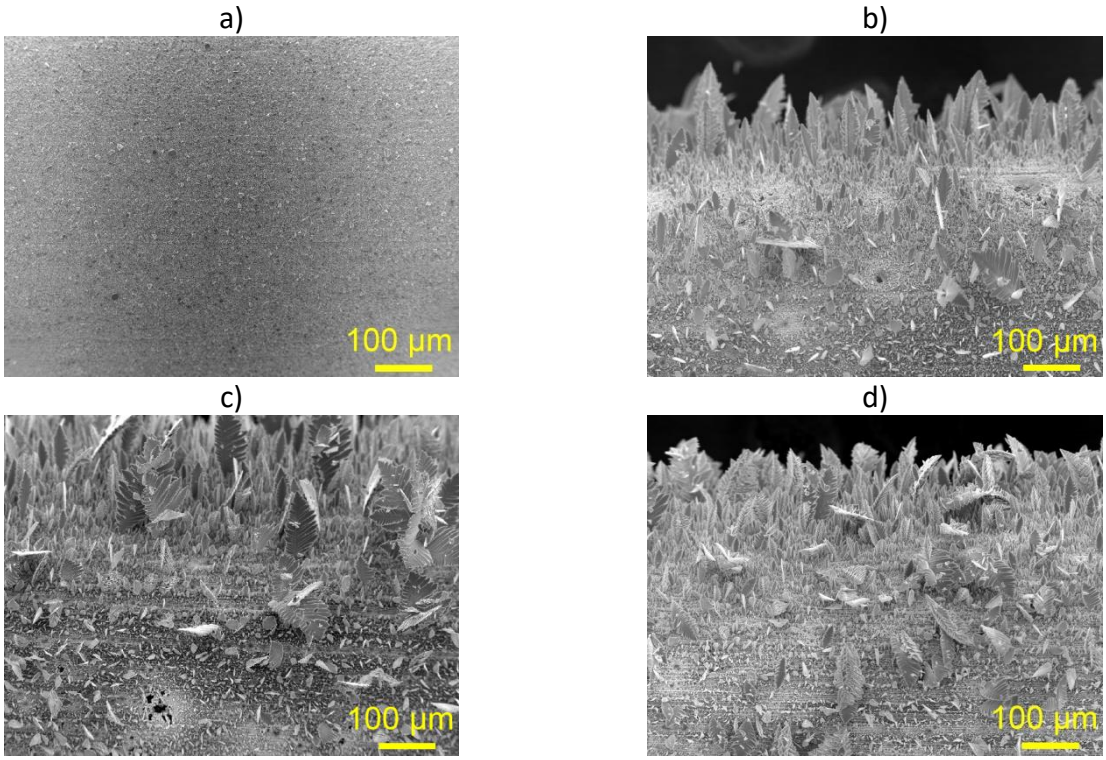

Figure 2. *The morphologies of Zn electrodeposits obtained at overpotentials of: (a) -160, (b) -220, (c) -280 and (d) -340 mV. The electrodeposited charge: 1.5 mAh. The surface area: 0.50 cm^2. Recorded at magnification 150×*

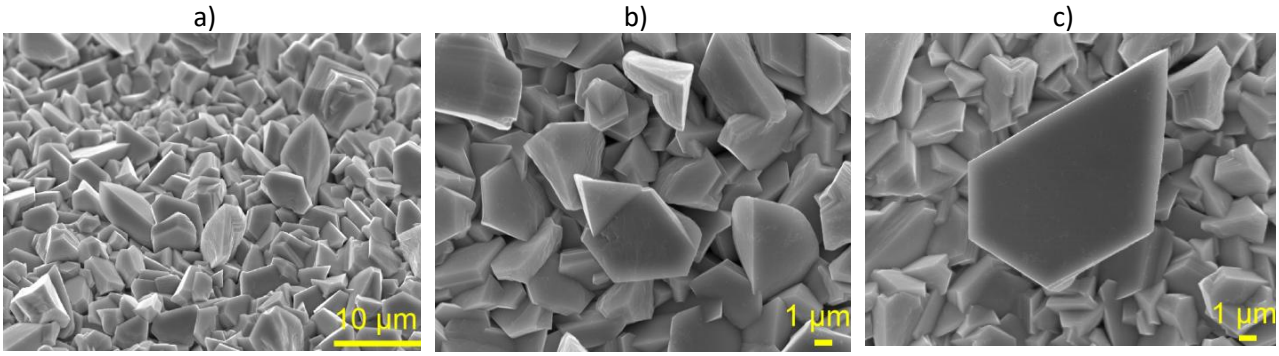

Figure 3. *The morphology of Zn deposit electrodeposited at an overpotential of -160 mV with an electrodeposited charge of 1.5 mAh. The surface area: 0.50 cm^2. Recorded at magnifications: (a) 2500×, (b) 5000× and (c) 5000×*

Detailed insight into the effect of overpotential electrodeposition on hole shape and size is obtained through additional analysis of Zn deposits produced at various overpotentials (Figures 4 to 6).

The morphology of the Zn deposit obtained at an overpotential of -220 mV is shown in Figure 4. The size of the holes formed at this overpotential was around 100 μm. The positions at which the hydrogen evolution reaction commences are clearly visible in Figure 4. The two-dimensional (2D) fern-like dendrites were predominantly formed around holes.

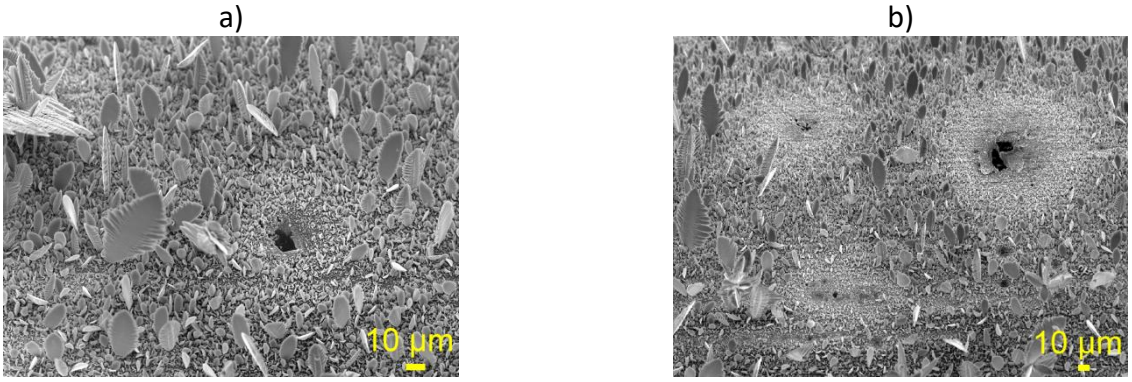

Figure 4. *The morphology of Zn deposit electrodeposited at an overpotential of -220 mV with an electrodeposited charge of 1.5 mAh. The surface area: 0.50 cm^2. Recorded at magnifications*: *(a) 500× and (b) 300×*

The holes formed during Zn electrodeposition at an overpotential of -280 mV are shown in Figure 5. The hole sizes were very different, ranging from 10 to 100 µm. The large holes like that shown in Figure 5b with the irregular bottom are obtained by a coalescence of closely formed hydrogen bubbles. The bottom of the hole itself is shown in Figure 5c. The mixture of the 2D fern-like and the three-dimensional (3D) dendrites was formed around the holes.

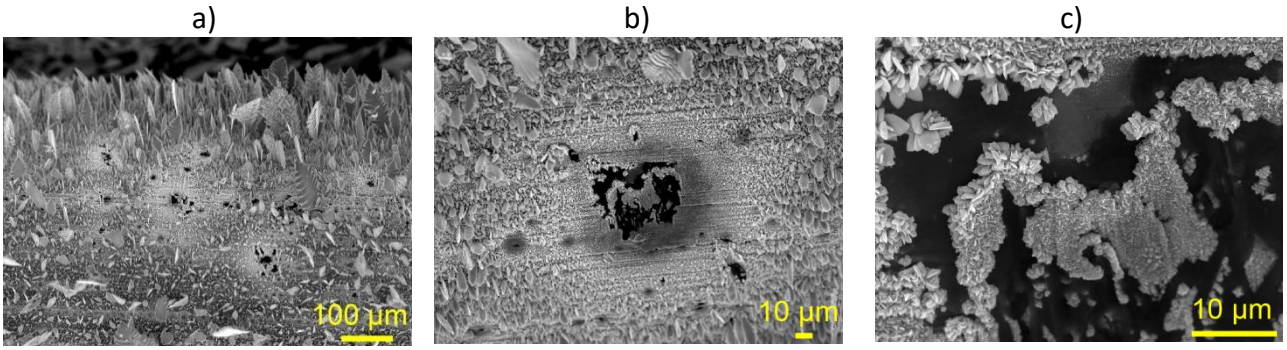

Figure 5*. The morphology of Zn deposit electrodeposited at an overpotential of -280 mV with an electrodeposited charge of 1.5 mAh. The surface area: 0.50 cm^2. Recorded at magnifications: (a) 150×, (b) 500× and (c) 2500×*

The morphology of the Zn deposit obtained at an overpotential of -340 mV, with a focus on holes originating from detached hydrogen bubbles, is shown in Figure 6.

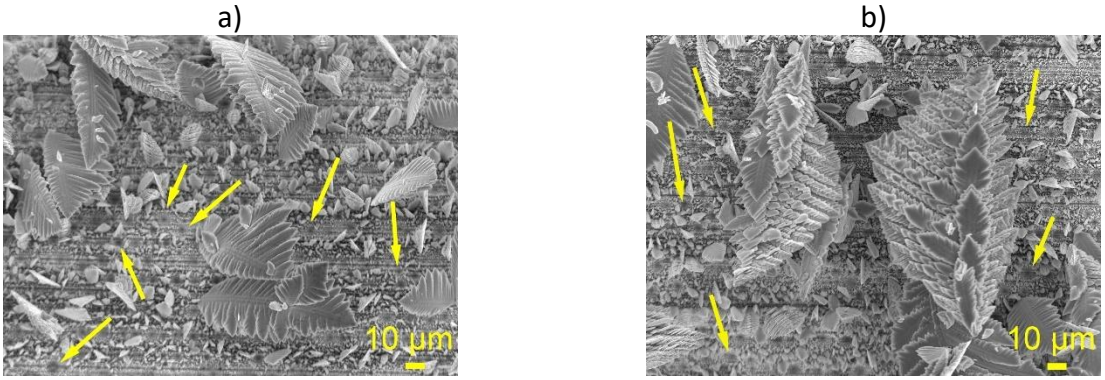

Figure 6. *The morphology of Zn deposit electrodeposited at an overpotential of -340 mV with an electrodeposited charge of 1.5 mAh. The surface area: 0.50 cm^2. Recorded at magnification 500×.*
SEM images (a) and (b) show different positions at the same electrodeposited surface with the aim to indicate a diversity of shape and size of the dendrites and the holes

The very small holes, less than 10 μm in size, can be identified in the morphology of this Zn deposit. Some of these holes are denoted by arrows in this Figure. The size of coalesced holes reached approximately 10 μm (Figure 6a). The very branchy, mainly 3D, dendrites formed around holes (Figure 6b).

The size of holes obtained at overpotentials of -220, -280 and -340 mV is included in Table 1.

The effect of electrodeposited charge on shape and size of holes

The additional insight into the formation of holes was obtained by analysis of the electrodeposition process at -280 and -340 mV with a double smaller electrodeposited charge (0.75 mAh). The initial stage of Zn electrodeposition at -280 mV with the electrodeposited charge of 0.75 mAh is shown in Figure 7a. Holes formed from detached hydrogen bubbles are clearly noticeable in this Zn deposit. The insight into the interior of one, about 100 μm large hole, revealed its irregular bottom (Figure 7b) around which numerous regular and irregular crystals (Figure 7c) similar to those obtained at an overpotential of -160 mV (Figure 3) are formed. The irregular bottom of this hole can be attributed to a coalescence of neighbouring initially formed hydrogen bubbles.

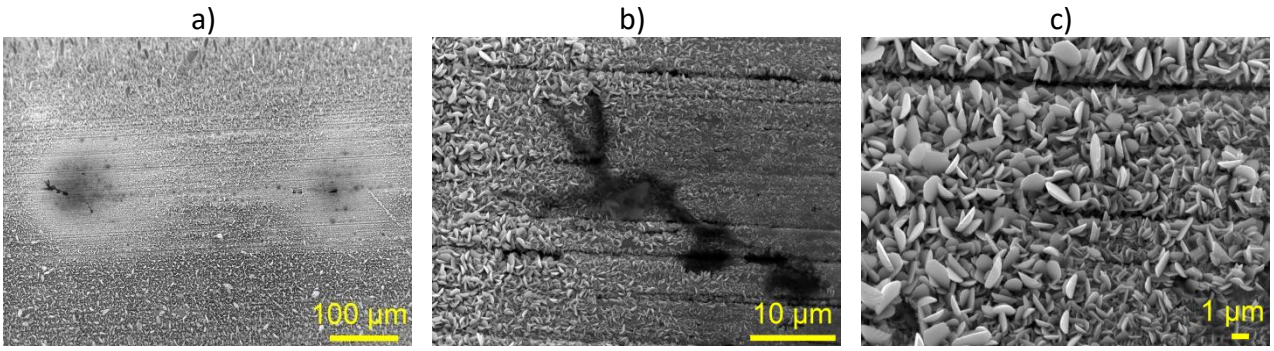

Figure 7. *The morphology of Zn deposit electrodeposited at an overpotential of -280 mV with an electrodeposited charge of 0.75 mAh. The surface area: 0.50 cm^2. Recorded at magnifications: (a) 200×, (b) 2500× and (c) 5000×*

The somewhat different situation was observed at -340 mV with an electrodeposited charge of 0.75 mAh (Figure 8). It can be noticed formation of a larger number of smaller holes occurs at this overpotential than at an overpotential of -280 mV (Figure 8a). The deeper analysis of one of the numerous holes clearly revealed its coalesced character (Figure 8b), with numerous dendrites formed around the bottom of the hole (Figure 8c). The size of the coalesced hole was about 10 μm, proving formation about 10 times smaller hole size at -340 than at -280 mV.

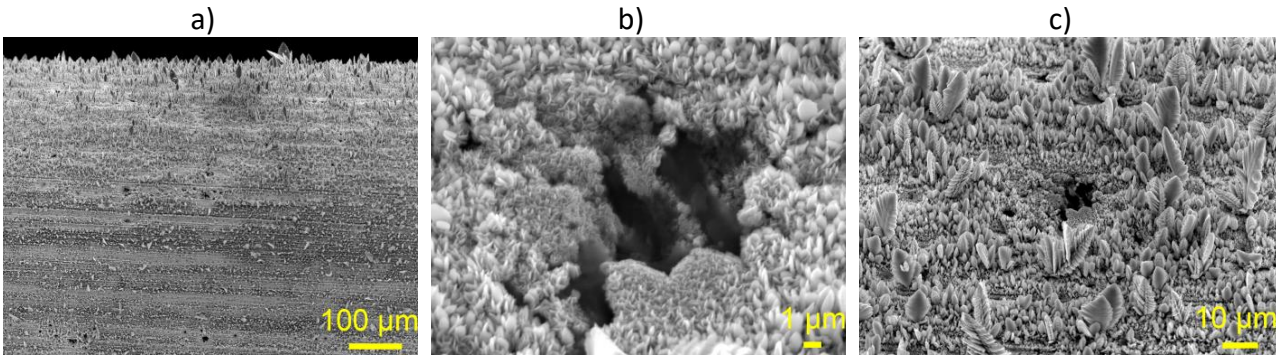

Figure 8. *The morphology of Zn deposit electrodeposited at an overpotential of -340 mV with an electrodeposited charge of 0.75 mAh. The surface area: 0.50 cm^2. Recorded at magnifications: (a) 150×, (b) 5000× and (c) 1000×*

Discussion of presented results

Analysis of Zn electrodeposition processes showed strong competition between Zn deposition and the hydrogen evolution reaction at overpotentials outside the plateau of the limiting diffusion current density. These two processes occur simultaneously, resulting in the formation of holes originating from detached hydrogen bubbles among the fast-growing 2D fern-like and 3D dendrites. Due to a parallel HER, the part of the electrode surface is blocked by growing hydrogen bubbles, and then the actual current density (*j*) can be given by Equation (6) [41]:

$$j = \frac{I / S}{1\text{-}\theta} \tag{6}$$

where *I* is the current of the electrodeposition, *S* is the surface area of the electrode, and θ is a fractional coverage of the electrode surface by hydrogen bubbles.

The two important phenomena can be mentioned by the analysis of the effect of HER on Zn electrodeposition process: (a) applied overpotential did not have any significant effect on the volume of generated hydrogen, since the current efficiency for HER were in a range between 17.7 and 19.1 %, and (b) the growth of dendrites was not inhibited by this relatively high volume of generated hydrogen.

Both Zn nucleation and HER commence on the most energetically active sites, such as irregularities on the electrode surface, and the number of these sites increases with increasing overpotential or current density during electrodeposition [42-44]. During electrodeposition, the hydrogen bubbles that form grow to a critical size, after which they detach from the electrode surface. During growth, neighbouring hydrogen bubbles coalesce, leading to larger holes in the deposit. The size of holes is a function of the electrodeposition overpotential, where a larger number of smaller holes is formed at higher than at lower overpotentials. In the case of Zn, the overall volume of evolved hydrogen remains approximately the same, while the increasing overpotential led to only re-distribution of formed holes, where a larger number of holes, but smaller in size is formed at higher (-340 mV) than at lower (-220 and -280 mV) overpotentials.

The decrease of the hole size with increasing the overpotential can be confirmed by the analysis of the break-off diameter, *d* as follows. The break-off diameter of a bubble can be defined by Equation (7):

$$\frac{d}{d_0} = \left(1 + 0.2\frac{I}{S}\right)^{-0.45} \tag{7}$$

where d_0 is a function of the surface tension, the density of electrolyte, and *I*/*S* is given in A m^{-2} [41,45]. Since the same electrolyte is used in all experiments, a contribution of d_0 in the value of the break-off diameter is the same at all overpotentials. Hence, the critical diameter of the hydrogen bubble that detaches from the electrode surface depends only on the electrodeposition overpotential.

In the potentiostatic mode of electrodeposition, the current is a function of time, as shown in Figure 9, which presents chronoamperograms obtained at overpotentials of -160, -220, -280, and -340 mV. For that reason, a relevant current in Equation (7) for this mode is an average current, I_{av} [45], which can be calculated from Equation (8), as:

$$I_{av} = \frac{\int_0^t I \mathrm{d}t}{t} \tag{8}$$

where *t* is the electrodeposition time to reach an electrodeposited charge $\int_0^t I \cdot \mathrm{d}t$.

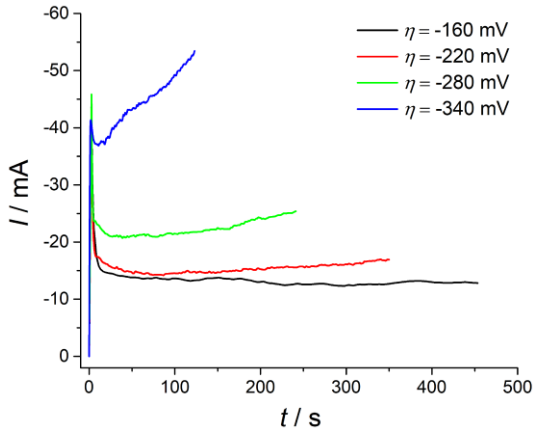

Figure 9. *The dependencies of* I - t *obtained at overpotentials of - 160, - 220, - 280, and - 340 mV. The surface area: 0.50 cm*^{2}

The calculated values of I_{av} obtained at overpotentials of-160, -220, -280 and -340 mV are added to Table 1. Analysis of Equation (7) with the values given in Table 1 confirms the decrease of the break-off diameter of the hydrogen bubble with increasing the overpotential of the electrodeposition, which is observed in this study.

It was very surprising that the pretty high volume of generated hydrogen did not cause an inhibition of dendritic growth, because an inhibition has already been observed with noticeably smaller volumes of evolved hydrogen during electrodeposition of copper at overpotentials outside the plateau of the limiting diffusion current density [22]. In the case of Cu, a volume of evolved hydrogen, which corresponded to a current efficiency for HER of approximately 10.0 %, was enough to inhibit the growth of dendrites. It was a minimum volume of evolved hydrogen that caused an effective stirring of the electrolyte in the near-electrode layer, leading to the decrease of the diffusion layer thickness and up to the increase of the limiting diffusion current density, resulting in the formation of the deposits without the dendrites [22].

To explain why dendritic growth is inhibited in the case of Cu, but not in the case of Zn, a classification of metals which takes into consideration key parameters in electrochemistry, such as the rate of electrochemical process (the exchange current density), melting point, and an overpotential for HER [46]. Depending on these parameters, metals are classified into three groups: *normal*, *intermediate* and *inert* metals. Zinc is situated, together with lead, silver, tin and cadmium into a group of *normal* metals. This group of metals is characterized by high exchange current densities (i_0 > 1 A dm^{-2}), low melting points, and high overpotentials for HER. The Zn properties, such as the exchange current density values in the (1.84 to 8.8 A dm^{-2}) range [23], formation of compact forms of both 2D fern-like and 3D dendrites and the appearance of parallel HER at overpotentials outside the plateau of the current density, unequivocally confirmed the belonging of Zn to the group of *normal* metals. On the other hand, copper belongs to the group of *intermediate* metals. They are characterized by medium values of the exchange current density (10^{-2} to 1 A dm^{-2}), and lower overpotentials for HER from the group of *normal* metals. For this group of metals, the evolution of hydrogen commences at the overpotential belonging to the plateau of the limiting diffusion current density and the shape of dendrites strongly differed from that characterizing the *normal* metals group (in the case of Cu, the 3D pine-like dendrites, constructed from approximately spherical grains, are formed).

Hence, it is clear that the rate of electrochemical process, *i.e*. the exchange current density, represents a key parameter determining the final morphology of electrodeposited metal, and gives

answers why dendritic growth is not inhibited in the case of Zn in spite of a relatively high volume of generated hydrogen. The electrochemical definition of dendrites predicts the formation of dendrites from a protrusion or an irregularity formed in an initial stage of electrodeposition and situated deeply inside the diffusion layer of the macroelectrode [22,23,35]. The protrusions or irregularities can be recognized among crystal grains formed at an overpotential of -160 mV (Figure 3). The transformation of some of the protrusions in the dendrites at overpotentials outside the plateau of the limiting diffusion current density will be prevented by growing hydrogen bubbles (Figure 7c; the part around the place where hydrogen evolution commenced). The tip of the protrusion grows under activation control, whereas the electrodeposition at the rest of the macroelectrode is predominantly diffusion-controlled. In fast electrochemical processes, such as Zn electrodeposition, activation-controlled tip growth of dendrites can disrupt the outer limit of the diffusion layer in a single moment [22,23,35]. At the polarization curve, the disruption of the diffusion layer is denoted by the beginning of a continuous growth of the current after the end of the plateau. Certainly, the effect of detached hydrogen bubbles on a convective flow of the electrolyte in the near-electrode layer cannot be neglected completely [36], but it is clear that their contribution to electrolyte mixing is not enough to inhibit dendritic growth. Due to the very high rate of the electrodeposition process, the fast-growing dendrites make barriers like tunnels, which only enable detached bubbles to move away from the electrode surface, without their influence on electrolyte mixing, which would lead to an inhibition of the growth of dendrites.

Conclusions

The electrodeposition of Zn from alkaline electrolytes, which plays a significant role in the development of Zn-based batteries, is considered. The analysis focused on the effect of parallel HER on the morphological characteristics of Zn deposits. The following conclusions were derived from the performed analysis of Zn electrodeposition processes:

- HER occurs at overpotentials outside the plateau of the limiting diffusion current density, while the eventual presence of this reaction does not lead to the formation of holes and craters within the plateau of the limiting diffusion current density.
- The overpotential of the electrodeposition did not show any significant effect on the evolution of hydrogen. The current efficiency for HER was in the range between 17.7 and 19.1 %.
- The overpotential of the electrodeposition strongly affected the size of the holes. Hole size decreased with increasing the overpotential of electrodeposition from about 100 to several μm.
- The growth of dendrites was not inhibited in spite of the relatively high volume of generated hydrogen. This unexpected behaviour was explained by the fact that Zn belongs to the group of *normal* metals, which are characterized by the high values of both the exchange current density and overpotential for the hydrogen evolution reaction.

Acknowledgements: *This work was supported by the Ministry of Science, Technological Development and Innovation of the Republic of Serbia (Contract No.: 451-03-136/2025-03/200026).*

References

[1] Y. Zuo, K. Wang, P. Pei, M. Wei, X. Liu, Y. Xiao, P. Zhang, Zinc dendrite growth and inhibition strategies, *Materials Today Energy* **20** (2021) 100692. https://doi.org/10.1016/j.mtener.2021.100692

[2] Z. Mandić, G. Mihalinec, X. Xin, M. Zhou, S. Burazer, Can the development of batteries keep pace with the ever-increasing demands of consumers?, *Journal of Electrochemical Science and Engineering* **15** (2025) 3120. https://doi.org/10.5599/jese.3120
[3] F. X. Xie, L. Zhang, C. Ye, M. Jaroniec, S. Z. Qiao, The application of hollow structured anodes for sodium-ion batteries: from simple to complex systems, *Advanced Materials* **31** (2019) 1800492. https://doi.org/10.1002/adma.201800492
[4] D. Kundu, B. D. Adams, V. Duffort, S. H. Vajargah, L. F. Nazar, A high-capacity and long-life aqueous rechargeable zinc battery using a metal oxide intercalation cathode, *Nature Energy* **1** (2016) 16119. https://doi.org/10.1038/nenergy.2016.119
[5] S. Liu, J. J. Hu, N. F. Yan, G. L. Pan, G. R. Li, X. P. Gao, Aluminum storage behavior of anatase TiO_2 nanotube arrays in aqueous solution for aluminum ion batteries, *Energy & Environmental Science* **5** (2012) 9743-9746. https://doi.org/10.1039/C2EE22987K
[6] B. Ji, F. Zhang, X. Song, Y. Tang, A novel potassium-ion-based dual-ion battery, *Advanced Materials* **29** (2017) 1700519. https://doi.org/10.1002/adma.201700519
[7] Y. Liu, L. Li, X. Ji, S. Cheng, Scientific Challenges and Improvement Strategies of Zn-Based Anodes for Aqueous Zn-Ion Batteries, *The Chemical Record* **22** (2022) e202200114. https://doi.org/10.1002/tcr.202200114.
[8] C. Li, L. Wang, J. Zhang, D. Zhang, J.Du,Y. Yao, G. Hon, Roadmap on the protective strategies of zinc anodes in aqueous electrolyte, *Energy Storage Materials* **44** (2022) 104-135. https://doi.org/10.1016/j.ensm.2021.10.020
[9] C. Wang, J. Li, Z. Zhou, Y. Pan, Z. Yu, Z. Pei, S. Zhao, L. Wei, Y. Chen, Rechargeable zinc-air batteries with neutral electrolytes: Recent advances, challenges, and prospects, *EnergyChem* **3** (2021) 100055. https://doi.org/10.1016/j.enchem.2021.100055
[10] F. W. Thomas Goh, Z. Liu, T. S. Andy Hor, J. Zhang, X. Ge, Y. Zong, A. Yu, W. Khoo, A Near-Neutral Chloride Electrolyte for Electrically Rechargeable Zinc-Air Batteries, *Journal of The Electrochemical Society* **161** (2014) A2080. https://doi.org/10.1149/2.0311414jes
[11] J. Hao, X. Li, S. Zhang, F. Yang, X. Zeng, S. Zhang, G. Bo, C. Wang, Z. Guo, Designing Dendrite-Free Zinc Anodes for Advanced Aqueous Zinc Batteries, *Advanced Functional Materials* **30** (2020) 2001263. https://doi.org/10.1002/adfm.202001263
[12] X. Zheng, T. Ahmad, W. Chen, Challenges and strategies on Zn electrodeposition for stable Zn-ion batteries, *Energy Storage Materials* **39** (2021) 365-394. https://doi.org/10.1016/j.ensm.2021.04.027
[13] X. Wang, C. Sun, Z.-S. Wu, Recent progress of dendrite-free stable zinc anodes for advanced zinc-based rechargeable batteries: Fundamentals, challenges, and perspectives, *SusMat* **3** (2023) 180-206. https://doi.org/10.1002/sus2.118
[14] N. Zdolšek, G. Mihalinec, F. Radovanović-Perić, D. Mikić, A. Dimitrijević, M. Kraljić Roković, Choline-based ionic liquid electrolyte additives for suppression of dendrite growth in Zn-ion batteries, *Journal of Electroanalytical Chemistry* **997** (2025) 119474. https://doi.org/10.1016/j.jelechem.2025.119474
[15] J. Fu, Z. P. Cano, M. G. Park, A. Yu, M. Fowler, Z. Chen, Electrically Rechargeable Zinc-Air Batteries: Progress, Challenges, and Perspectives, *Advanced Materials* **29** (2017) 1604685. https://doi.org/10.1002/adma.201604685
[16] K. Wang, Solutions for Dendrite Growth of Electrodeposited Zinc, *ACS Omega* **5** (2020) 10225-10227. https://doi.org/10.1021/acsomega.0c01485
[17] B. Li, X. Zhang, T. Wang, Z. He, B. Lu, S. Liang, J. Zhou, Interfacial engineering strategy for high-performance Zn metal anodes, *Nano-Micro Letters* **14** (2021)6. https://doi.org/10.1007/s40820-021-00764-7
[18] Y. Li, H. Dai, Recent advances in zinc-air batteries, *Chemical Society Review* **43** (2014) 5257-5275. https://doi.org/10.1039/C4CS00015C

[19] C. Li, X. Xie, S. Liang, J. Zhou, Issues and future perspective on zinc metal anode for rechargeable aqueous zinc-ion batteries, *Energy & Environmental Materials* **3** (2020) 146-159. https://doi.org/10.1002/eem2.12067.
[20] K. Bogomolov, Y. Ein-Eli, Alkaline Ni-Zn Rechargeable Batteries for Sustainable Energy Storage: Battery Components, Deterioration Mechanisms, and Impact of Additives, *ChemSusChem* **17** (2023) e202300940. https://doi.org/10.1002/cssc.202300940
[21] P. Pei, K. Wang, Z. Ma, Technologies for extending zinc-air battery's cyclelife: A review, *Applied Energy* **128** (2014) 315-324. https://doi.org/10.1016/j.apenergy.2014.04.095
[22] K. I. Popov, S. S. Djokić, N. D. Nikolić, V. D. Jović, *Morphology of Electrochemically and Chemically Deposited Metals,* Springer, New York, NY, USA, 2016. https://doi.org/10.1007/978-3-319-26073-0
[23] N. D. Nikolić, P. M. Živković, J. D. Lović, G. Branković, Application of the general theory of disperse deposits formation in an investigation of mechanism of zinc electrodeposition from the alkaline electrolytes, *Journal of Electroanalytical Chemistry* **785** (2017) 65-74. https://doi.org/10.1016/j.jelechem.2016.12.024
[24] V. S. Nikitin, T. N. Ostanina, V. M. Rudoi, T. S. Kuloshvili, A. B. Darintseva, Features of Hydrogen Evolution during Electrodeposition of Loose Deposits of Copper, Nickel and Zinc, *Journal of Electroanalytical Chemistry* **870** (2020) 114230. https://doi.org/10.1016/j.jelechem.2020.114230
[25] T. N. Ostanina, V. M. Rudoi, V. S. Nikitin, A. B. Darintseva, S. L. Demakov, Change in the physical characteristics of the dendritic zinc deposits in the stationary and pulsating electrolysis, *Journal of Electroanalytical Chemistry* **784** (2017) 13-24. https://doi.org/10.1016/j.jelechem.2016.11.063
[26] T. N. Ostanina, V. M. Rudoi, A. V. Patrushev, A. B. Darintseva, A. S. Farlenkov, Modelling the Dynamic Growth of Copper and Zinc Dendritic Deposits under the Galvanostatic Electrolysis Conditions, *Journal of Electroanalytical Chemistry* **750**(2015) 9-18. https://doi.org/10.1016/j.jelechem.2015.04.031
[27] N. D. Nikolić, J. D. Lović, V. M. Maksimović, N. S. Vuković, N. L. Ignjatović, P. M. Živković, S. I. Stevanović, Correlation Between Morphology and Crystal Structure of Electrolytically Produced Zinc Dendritic Particles, *Metals* **14** (2024) 1468. https://doi.org/10.3390/met14121468
[28] N. D. Nikolić, J. D. Lović, V. M. Maksimović, N. S. Vuković, P. M. Živković, The preferred orientation of electrodeposited dendrites of lead, tin and zinc, *Journal of Electrochemical Science and Engineering* **15** (2025) 2671. https://doi.org/10.5599/jese.2671
[29] V. Jabbari, T. Foroozan, R. Shahbazian-Yassar, Dendritic Zn Deposition in Zinc-Metal Batteries and Mitigation Strategies, *Advanced Energy & Sustainability Research***2** (2021) 2000082. https://doi.org/10.1002/aesr.202000082
[30] S. J. Banik, R. Akolkar, Suppressing Dendritic Growth during Alkaline Zinc Electrodeposition using Polyethylenimine Additive, *Electrochimica Acta* **179** (2015) 475-481. https://doi.org/10.1016/j.electacta.2014.12.100
[31] J. W. Diggle, A. R. Despic, J. O' M. Bockris, Mechanism of dendritic electrocrystallization of zinc, *Journal of The Electrochemical Society* **116** (1969) 1503-1514. DOI:10.1149/1.2411588
[32] M. Matsushita, M. Sano, Y. Hayakawa, H. Honjo, Y. Sawada, Fractal structures of zinc metal leaves grown by electrodeposition, *Physical Review Letters* **53** (1984) 286. https://doi.org/10.1103/PhysRevLett.53.286
[33] A. A. Wheeler, B. T. Murray, R. J. Schaefer, Computation of dendrites using a phase field model, *Physica D: Nonlinear Phenomena* **66** (1993) 243-262. https://doi.org/10.1016/0167-2789(93)90242-S

[34] D. A. Cogswell, Quantitative phase-field modeling of dendritic electrodeposition, *Physical Review E* **92** (2015) 011301. https://doi.org/10.1103/PhysRevE.92.011301
[35] K. I. Popov, N. D. Nikolić, *General Theory of Disperse Metal Electrodeposits Formation i*n *Electrochemical Production of Metal Powders, Series: Modern Aspects of Electrochemistry, Volume 54*, S.S. Djokić, Ed., Springer, New York, NY, USA, 2012, pp. 1-62. https://doi.org/10.1007/978-1-4614-2380-5_1
[36] J. Dundálek, I. Šnajdr, O. Libánský, J. Vrána, J. Pocedič, P. Mazúr, J. Kosek, Zinc electrodeposition from flowing alkaline zincate solutions: Role of hydrogen evolution reaction, *Journal of Power Sources* **372** (2017) 221-226. https://doi.org/10.1016/j.jpowsour.2017.10.077
[37] R. E. F. Einerhand, W. H. M. Visscher, E. Barendrecht, Hydrogen production during zinc deposition from alkaline zincate solutions, *Journal of Applied Electrochemistry* **18** (1988) 799-806. https://doi.org/10.1007/BF01016034
[38] Y. He, Y. Liu, W. Shang, P. Tan, Hydrogen bubble evolution and its induced mass transfer on zinc electrodes in alkaline and neutral media, *Nanoscale* **17** (2025) 8453-8465. https://doi.org/10.1039/D4NR05108D
[39] P.-C. Hsu, S.-K. Seol, T.-N. Lo, C.-J. Liu, C.-L. Wang, C.-S. Lin, Y. Hwu, C. H. Chen, L.-W. Chang, J. H. Je, G. Margaritondo, Hydrogen Bubbles and the Growth Morphology of Ramified Zinc by Electrodeposition, *Journal of The Electrochemical Society* **155** (2008) D400-D407. https://doi.org/10.1149/1.2894189
[40] B. Sharifi, M. Mojtahedi, M. Goodarzi, J. Vahdati Khaki, Effect of alkaline electrolysis conditions on current efficiency and morphology of zinc powder, *Hydrometallurgy* **99** (2009) 72-76. https://doi.org/10.1016/j.hydromet.2009.07.003
[41] H. Vogt, R. J. Balzer, The bubble coverage of gas-evolving electrodes in stagnant electrolytes, *Electrochimica Acta* **50** (2005) 2073-2079. https://doi.org/10.1016/j.electacta.2004.09.025
[42] N. D. Nikolić, K. I. Popov, Lj. J. Pavlović, M. G. Pavlović, Phenomenology of a formation of a honeycomb - like structure during copper electrodeposition, *Journal of Solid State Electrochemistry* **11** (2007) 667-675. https://doi.org/10.1007/s10008-006-0222-z
[43] L. J. J. Janssen, J. G. Hoogland, The effect of electrolytically evolved gas bubbles on the thickness of the diffusion layer, *Electrochimica Acta* **15** (1970) 1013-1023. https://doi.org/10.1016/0013-4686(70)80041-X
[44] J. P. Glas, J. W. Westwater, Measurements of the growth of electrolytic bubbles, *International Journal of Heat and Mass Transfer* **7** (1964) 1427-1430. https://doi.org/10.1016/0017-9310(64)90130-9
[45] N. D. Nikolić, G. Branković, M. G. Pavlović, K. I. Popov, The effect of hydrogen codeposition on the morphology of copper electrodeposits. II. Correlation between the properties of electrolytic solutions and the quantity of evolved hydrogen, *Journal of Electroanalytical Chemistry* **621** (2008) 13-21. https://doi.org/10.1016/j.jelechem.2008.04.006
[46] R. Winand, Electrodeposition of Metals and Alloys-New Results and Perspectives, *Electrochimica Acta* **39** (1994) 1091-1105. https://doi.org/10.1016/0013-4686(94)E0023-S